Three-dimensional confocal microscopy of colloids

A. D. Dinsmore, Eric R. Weeks, Vikram Prasad, Andrew C. Levitt, and D. A. Weitz

Confocal microscopy is used in the study of colloidal gels, glasses, and binary fluids. We measure the three-dimensional positions of colloidal particles with a precision of approximately 50 nm (a small fraction of each particle's radius) and with a time resolution sufficient for tracking the thermal motions of several thousand particles at once. This information allows us to characterize the structure and the dynamics of these materials in qualitatively new ways, for example, by quantifying the topology of chains and clusters of particles as well as by measuring the spatial correlations between particles with high mobilities. We describe our experimental technique and describe measurements that complement the results of light scattering. © 2001 Optical Society of America

OCIS codes: 110.2960, 110.0180, 180.1790.

1. Introduction

The dynamic and the structural properties of colloidal suspensions have been of intense interest for decades, owing to their industrial and biomedical importance. Colloids are commonly found, e.g., in coatings, foods, and cosmetics, whose rheological properties are central to the application. In addition, model colloidal suspensions provide uniquely powerful insight into fundamental problems such as crystallization, glass transition, kinetics of gelation, and structure of fluids. For many years light scattering has provided quantitative characterization of the average structure and dynamics of suspended particles. An advantage of scattering techniques is that they average over a large ensemble, so measurements can be fast and statistical uncertainties small. In many systems, however, it is not enough to know what the averaged properties are to be able to understand their behavior: A few mobile particles might dictate the aging properties of the material, for example, or a small density of structurally weak configurations might dominate the viscoelasticity. Structural and dynamic heterogeneities typically cannot be detected and spatially mapped with light scattering.

With confocal microscopy structure and motions can be measured precisely in three dimensions with single-particle resolution and no averaging. The key to the technique is the use of a pinhole aperture that is confocal with the image point. The aperture blocks light from other points in the sample and permits the imaging of a unique, well-defined spot deep inside the sample. By scanning this spot (typically with moving mirrors and motion of the objective for the third dimension), one can construct a a three-dimensional image.

Techniques for confocal microscopy have been under active development for more than a decade. Several novel techniques were, in fact, reviewed in a feature on microscopy in this journal in 1994.[1] The use of a confocal microscope in colloid physics, however, requires specialized samples and, in particular, the development of powerful image-analysis algorithms. The ability to measure the precise three-dimensional positions of millions of particles was therefore developed more recently[2,3] (see the 1997 review by Chestnut,[4] for example). Here we describe our techniques for sample preparation, data acquisition, and image analysis. The image-acquisition routines described here can sample of the order of 10^4 particles in 10 s or less. This fast scan rate permits studies of particle dynamics that have not been possible with other confocal systems. In addition, the particles are neutrally buoyant, so sedimentation is largely eliminated, and we can study aging over many days.

Confocal microscope measurements have provided powerful insight into many types of colloidal mate-

0003-6935/01/244152-08$15.00/0

rial. Van Blaaderen and Wiltzius[2] applied this technique to study the structure and bond symmetry of colloidal glass. More recently, Kegel and van Blaaderen[5] and Weeks *et al.*[3] observed dynamic inhomogeneities in colloidal glass in two and three dimensions, respectively. Confocal microscopy has also been used to study the structure of electrorheological fluids[6] and colloidal crystals grown upon templates.[7,8] Fractures in colloidal gels have also been observed,[9] although without single-particle resolution. In this paper, we focus on colloidal gels, colloidal glasses, and binary colloidal fluids. In each of these cases, we show how these measurements provide qualitatively new understanding of colloidal aggregation and phase transitions. For gels and dense binary fluids the confocal microscope permits unique insight into the structural heterogeneities of the material. For colloidal glass, we use the microscope to study dynamic heterogeneities by simultaneously measuring the positions and the mobilities of individual particles.

2. Experimental Procedure

To achieve high resolution and background rejection in concentrated suspensions, we used a confocal microscope (Noran Instruments Model Oz) operating in fluorescence mode. The confocal microscope was mounted upon a Leica Model DMIRB inverted microscope base equipped with an oil-coupled Leica plan apochromat objective with a $100\times$ magnification and a numerical aperture of 1.4. Fluorescence from the sample was excited with the 488-nm line of an Ar laser. The fluorescence was separated from the excitation light by a dichroic beam splitter and a long-pass filter with a cutoff wavelength of 500 nm. The microscope objective was attached to a piezoelectric driver (Physik Instrumente) to scan the objective along the vertical z direction and produce three-dimensional images. This confocal microscope acquires images at an unusually fast rate because it scans the beam quickly along one dimension, using an acousto-optic deflector. The fast scan requires the use of a slit, rather than the conventional pinhole, to reject the out-of-plane light. In our samples, however, the slit and the slight image anisotropy that it causes did not significantly affect the precision of particle-position measurements, which was approximately 50 nm. The acquisition time for each 512×480 pixel slice in the horizontal x–y plane was typically 1/30 s, although much faster acquisition is possible at lower resolution or with a reduced field of view. The edge of the typical full-sized field of view is approximately 45 μm.

We typically acquired stacks of 50–100 images separated by 0.1 μm or more in the z direction. Acquisition of a full three-dimensional stack of images required approximately 4–10 s. When we were monitoring 1-μm particles undergoing free diffusion, we could track the particles in two dimensions, but the three-dimensional scanning was too slow to follow individual particles at volume fractions of 0.03 or greater, which is the range of volume fractions discussed here. When the particles slowed down, either because of aggregation or when the volume fraction exceeded approximately 0.50, we could track the particles even when we were performing a full three-dimensional scan. We chose a solvent to match the refractive index of the particles so that we could look 100 μm or more into the sample without noticeable loss of resolution. The penetration depth was limited by the microscope objective, not by the scattering of light.

The samples contained monodisperse poly(methyl methacrylate) (PMMA) spheres, which were synthesized by A. Schofield, P. Pusey, and their co-workers at the University of Edinburgh. These particles were coated with a layer of hydroxystearic acid for steric stabilization in a suspension of organic fluid. We incorporated rhodamine fluorescent dye within the particles by using the following procedure[3]: We prepared a solution of 25 vol. % acetone and 75 vol. % cyclohexanone in 1 mg/ml of rhodamine perchlorate. We added 1 ml of this solution dropwise, while stirring, to 2 ml of dodecane with PMMA beads (volume fraction ϕ, approximately 0.10). This solution was then mixed thoroughly until the color changed from purple to orange (typically within 20 min), after which we centrifuged the solution, decanted the supernatant, and resuspended the particles in decalin (decahydronaphthalene, 98%; Aldrich Company, Milwaukee, Wisconsin). We repeated the washing step at least 10 times over the following 2 weeks. Finally, cycloheptyl bromide (CHB, 97%; Aldrich) or cyclohexyl bromide (CXB, 98%; Aldrich) was added to the solution to match the mass density of the particles to that of the solvent. (CHB is compatible with the polystyrene polymer, which we used in some experiments, but CXB is probably more stable over a period of several months.) We improved the density matching by centrifuging the solution at 6000 g, noting whether the particles settled upward or downward, and adding the appropriate solvent. We repeated this process over a period of a month until no sedimentation was observed after centrifuging for at least 15 h. The density of the particles decreased slightly over several days owing to a slight swelling of the particle radius. To determine the composition of the density-matched solvent, we followed the same routine with a very dilute suspension ($\phi < 10^{-6}$) and weighed the amounts of solvent added. We found that the mass density of the final neutrally buoyant decalin–CHB mixture was 1.220 g/ml.

The interactions among the undyed PMMA spheres are well approximated by a hard-sphere potential.[10,11] We found, however, that the process of incorporating dye into the particles introduces some electrostatic repulsion. Although the interaction energy is weak (probably $< k_B T$ near contact), the repulsion length is probably very long ($\gg 1$ μm) owing to the low dielectric constant and the low concentration of free ions in the organic solvent. As a result, we observed freezing points in dyed samples at volume fractions greater than approximately 0.4,

which is below the hard-sphere freezing point at 0.494.

To study colloidal aggregates (gels), we induced a controllable attraction among the particles by the addition of a nonadsorbing polymer.[9,12] The polymer induces depletion forces that squeeze the PMMA particles together whenever their surfaces approach closely enough to exclude a polymer molecule.[13,14] The spatial range of attraction is approximately twice the polymer's radius of gyration R_g. The energy of attraction U is well approximated by $U = 1.5k_BT(R/R_g)(c_pN_A/M)(4\pi R_g{}^3/3)$, where R is the PMMA sphere radius, M is the molecular weight of the polymer, N_A is Avogadro's number, c_p is the concentration of polymer (mass per volume of solution), and k_BT is Boltzmann's constant times the absolute temperature. The last two factors in the equation are the volume fraction of the polymer, which sets the osmotic pressure that squeezes the particles together.

Solutions of polymeric polystyrene ($M = 1.95 \times 10^6$ g/mol and $R_g = 35$ nm; Polymer Laboratories, Inc.) were prepared by use of the same mix of decalin and CHB as was used for the particles (for the gel studies $R = 0.35$ μm). We allowed at least 3 days for the polystyrene polymer to swell in the solvent. By mixing the particle suspension with the polymer solution and a pure mixture of CHB and decalin, we could vary the particle volume fraction φ as well as U, while preserving the density match with the solvent. In all samples discussed here the final polymer concentration was less than the overlap concentration. We carried out these experiments by first shaking the samples vigorously by hand and then verifying with the microscope that the particles were well separated. We then acquired images periodically and at various positions in the sample over as many as 4 days without disturbing the samples. Over a period of approximately 40 h there was no evidence of sedimentation: The density appeared to be uniform along the vertical axis. After 90 h, however, we could see an approximately 1.5% decrease in density over a depth of 50 μm.

In all experiments, we analyzed the images by using the Interactive Data Language programming environment on a Pentium II computer with the Linux operating system. We used routines written by David G. Grier, John C. Crocker, and Eric R. Weeks for the spatial filtering of images and the precise determination of three-dimensional particle positions[15] (see the website http://glinda.lrsm. upenn.edu/~weeks/idl/ for details of these algorithms). The uncertainty of the particle coordinates is approximately 50 nm, which is approximately half a pixel. The resolution is limited principally by movement of the particles, which typically appeared in approximately 10 consecutive slices whose acquisition required 0.5 s or more. Obtaining a list of all of the x, the y and the z coordinates of 5000 particles in a stack of 60 images required approximately 15 min. We used these lists of parti-
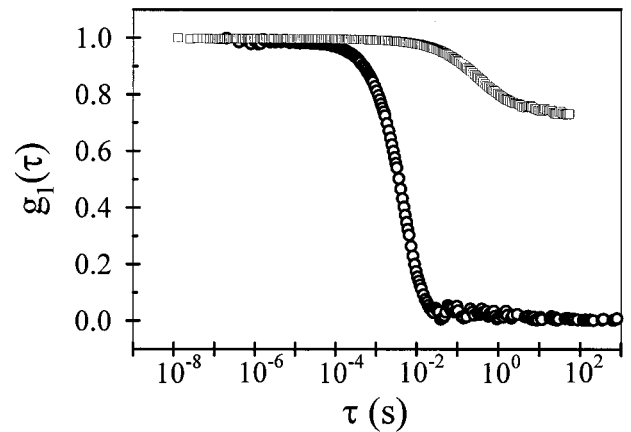

Fig. 1. Plot of the field autocorrelation functions of light scattered from two colloidal suspensions. Open circles, colloidal fluid (φ = 0.02, $U = 0$); open squares, colloidal gel (φ = 0.085, $U = 16.5\ k_BT$, $R_g/R = 0.06$). The scattering angle is 60° ($q = 1.8 \times 10^5$ cm^{-1}), which lies between the high-q and the low-q peaks in the structure factor of the gel.

cle positions to quantify the structure of the colloids in ways that are discussed below.

3. Results

A. Colloidal Gels

In the absence of polystyrene polymer ($U = 0$) a dilute suspension of PMMA particles does not aggregate—it is considered a colloidal fluid. When U is increased to approximately $5\ k_BT$ by the addition of polymer the particles aggregate and form a random structure known as a gel, which is a weak solid. Mixtures of colloidal particles and polymer provide a model system with which to study this fluid–solid transition: The interactions among the particles can be controlled by means of the polymer size R_g and concentration.

Dynamic light scattering provides quantitative measurements of the mobility of particles in the sample and can be used to distinguish samples that form a gel. Figure 1 shows the temporal autocorrelation function $g_1(\tau)$ of the light scattered from two colloidal suspensions at an angle of 60° ($q = 1.8 \times 10^5$ cm^{-1}). In both samples the particle radius was 136 nm. The open circles correspond to a sample with a volume fraction of φ = 0.02. The correlation function decays exponentially to zero, as is characteristic of diffusing particles. The squares correspond to a sample with φ = 0.085 and with polymer added ($U = 16.5\ k_BT$ and $R_g/R = 0.06$). Here the correlation function decays by only 25% over 1000 s and has a much longer decay time. This behavior is characteristic of a solid (here, a gel). Dynamic light scattering can therefore be used as a probe to distinguish fluid samples from gels.[16–18]

We focus here on a sample that forms a gel. After the sample is shaken to randomize the particle positions and break up aggregates the particles begin to aggregate by diffusion-limited cluster aggregation.[19,20]
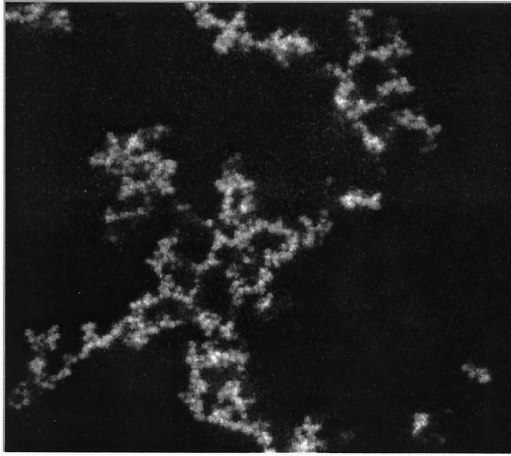
Fig. 2. Confocal microscope image of a colloidal gel. The image is a projection over a depth of 1.6 μm. The particles, visible as white spots, are 0.35 μm in radius, and φ = 0.031. The polystyrene polymers, which make the particles aggregate ($U = 8.4\,k_BT$), are not visible.
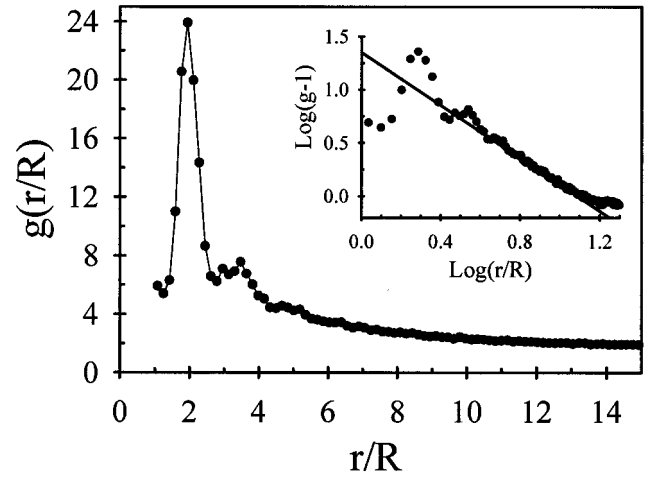

Fig. 3. Pair distribution function $g(r)$ of a colloidal gel, measured by three-dimensional confocal imaging; r is the distance from the center of a particle, and R is the particle radius. The sample is the same as in Fig. 2, and the data are averaged over 20,000 particles. Inset, log–log plot of the same data, showing power-law scaling. The line has a slope of −1.24, which leads to a fractal dimension $D_f = 1.76$. The peaks near the origin are due to bonding with other particles.

We verified that the mean cluster size initially increases linearly with time, and dynamic scaling of the cluster size distribution was observed.[21–23] After approximately 10 h all the particles formed one single cluster, which spanned the sample and thus was termed a gel.

Figure 2 shows a confocal microscope image of the gel 90 h after stirring. This image is a projection over a depth of 1.6 μm, or 4.5 particle radii (nine image slices). The volume fraction of the spheres φ was 0.031, and the interaction energy that is due to depletion U was 8.4 k_BT. The random nature of the structure is visible: There is no long-range order. At first glance the structure appears to be composed of long chains of aggregated particles that propagate in three dimensions. These chains allow the structure to resist shear stress; it behaves as a solid when it is subjected to weak, low-frequency shear. Our goal was to characterize the structure of this gel and relate the structure to the gel's viscoelasticity. With microscope images such as these, we measured particle positions and obtained a new description of the gel's structure.

Figure 3 shows the pair distribution function $g(r)$ for this sample plotted as a function of the normalized separation r/R, where the particle radius is $R = 0.35$ μm. The function $g(r)dr$ is proportional to the probability of finding a particle located in a shell of radius r and thickness dr about a particle at the origin (normalized by the volume of the shell). The plot was obtained from measurements of the positions of 20,000 particles. There are peaks at small r that correspond to bonding to the nearest and the next-nearest neighbors. At $4R < r < 15R$ there is power-law scaling that is due to fractal scaling of the density: $g(r) - 1 \propto r^{3-D_f}$, where D_f is the fractal dimension. From the inset of Fig. 3, we obtained $D_f = 1.76$. We measured the same fractal dimension from the scaling of the cluster mass M_{clus} with the

cluster radius of gyration R_{clus} during aggregation.[24] In the measured pair distribution function the fractal scaling is lost when $r > 15R$. This upper cutoff of the fractal scaling, approximately $15R$, is known as the correlation length R_c and is related to the volume fraction by a simple estimate: $R_c/R = \phi^{1/(D_f-3)} = 16.5$. These features are also seen in light-scattering measurements and provide the structure factor[20,25] [the Fourier transform of $g(r)-1$]. The scattering measurements, however, leave out much information about the detailed structure of the gel. At intermediate values of r, for example, the function $g(r)$ does not indicate whether the particles are arranged in chains, what the sizes of these chains are, or whether loops are present.

Using confocal microscopy, we measured the number of bonds per particle. Particles were considered to be bonded if their measured center-to-center separation fell below a cutoff value r_c. We defined r_c as the location of the first minimum of the pair distribution function and noted that it agreed with the expected value, which is $2(R + R_g)$, the range of the depletion attraction. A particle's bond number n_b was defined as the number of bonds that the particle formed with its neighbors. We determined distributions of n_b by looking at all particles within the clusters of a given mass. This approach accounts for the observation that the mean bond number increases slightly with the cluster mass because a smaller fraction of particles resides at the cluster's surface.

Figure 4 shows the distribution of bond numbers n_b for the same sample as was used for Figs. 2 and 3. These measurements were made after the gel had formed, 21 h after stirring. The bonds about 7335 particles are included in this plot. The distribution did not change substantially with time from 5 h (pre-
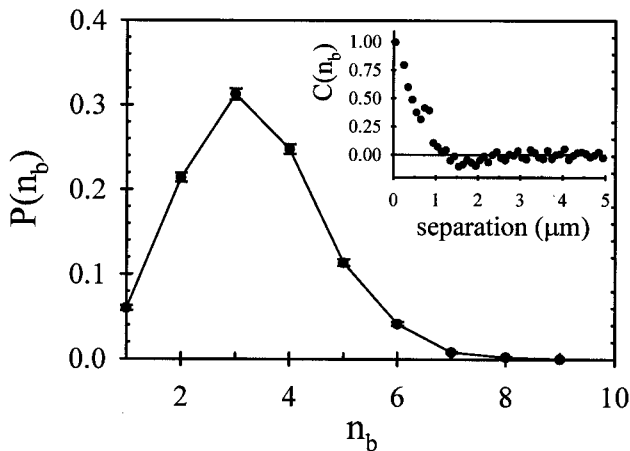
Fig. 4. Distribution of the number of bonds per particle n_b obtained by three-dimensional confocal imaging. This is the same sample as in Fig. 2; 7335 particles are included in this plot. Inset, spatial correlation of n_b versus separation between particles ($R = 0.35 \mu m$); 1300 particles are included in this plot. The lack of significant correlation beyond nearest neighbors indicates the absence of a characteristic mesh size, of long, single chains, or of a chain–blob morphology.

gelling) to 90 h, although there is a systematic decrease in $P(n_b \leq 3)$ and an increase in $P(n_b \geq 4)$ over time. Just slightly more than 20% of the particles have a bond number of $n_b = 2$, which is characteristic of a single-file chain. Breaking one of these bonds is likely to break the chain of particles. Inasmuch as the particles with just two bonds should be the weakest members of the chain, their number density may significantly affect the strength of the gel as a whole. [The cover illustration shows a three-dimensional reconstruction of a section of this sample (aged 90 h). The colors in this illustration indicate the measured number of bonds per particle.]

Measurements of the bond-number distribution thus provide an estimate of how many bonds must be broken to break a chain and permit structural relaxation. This information is necessary for the understanding of aging and rheology, which are the responses of the material to thermal fluctuations and external stress. Indeed, recent models[26,27] of the frequency dependence of a complex shear modulus rely on an estimate of the number of bonds that must be broken to sever a chain and allow it to move. To our knowledge these confocal microscope images provide the first experimental probes of these properties.

Approximately 40% of the particles in the gel have four bonds or more, suggesting that there might be nodes, or blobs, distributed throughout the structure. Such blobs would be characterized by a clump of particles, all with a value of n_b that is above average. To see whether such was the case, we looked at the spatial distribution of n_b. Specifically, we calculated $C(r)$, the mean correlation of the bond numbers of two particles that are separated by a distance r (see Fig. 4, inset). A value of $C(r) = 1$ indicates perfect correlation, $C(r) = 0$ indicates no correlation, and $C(r) = -1$ indicates anticorrelation. Because nearest

neighbors share a bond, n_b is weakly correlated over the distance of a particle diameter. The bond numbers, however, have nearly zero correlation beyond the nearest-neighbor distance, indicating that the structure does not form long chains, which would maintain the correlation of n_b over a long distance. The slight anticorrelation at $r = 2 \mu m$ hints at blobs of particles that are connected by chains; such a structure would show anticorrelation over an intermediate-length scale. The measured anticorrelation, however, is quite weak, suggesting that the blob-and-chain picture is not appropriate.

To obtain a more precise picture of the gel's structure, we searched for closed loops of particles. To find loops, we first searched for particles that form pivot points in the gel. These pivot points were defined as those places where breaking a single bond would completely sever the chain. At each pivot point, we began stepping along the chain in one direction. The length of the loop was then defined as the minimum number of steps needed to return to the pivot point without backtracking. If we reached the end of the field of view, we reported no measurement and moved to the next pivot point. A plot of the distribution of loop lengths reveals power-law scaling with an exponent of -1.7 to -2, similar to the fractal dimension. There are loops and chains of all lengths with no characteristic length scale and no mesh size. These observations suggest that the viscoelasticity of the gel might not be described accurately with a model that accounts only for single chains; loops and cross links might have to be included.

B. Concentrated Binary Suspensions

We also studied the structure of suspensions of spheres of two different sizes. In dilute binary mixtures, as discussed in Subsection 3.A, the small particles can induce an attraction between the larger particles as a result of depletion. Crocker et al.[14] recently measured the depletion potential between two hard spheres in the presence of much smaller spheres (ratio of diameters, 0.088). When the volume fractions of the smaller spheres ϕ_S was less than 0.1, the interaction was purely attractive and was well described by the assumption that the small spheres were an ideal gas. We used this approximation in Subsection 3.A to derive the strength of the depletion force in the colloid–polymer gels. A high concentration of small particles, however, can *prevent* aggregation of the larger particles. Crocker et al. found that, when ϕ_S exceeded 0.1, a repulsion barrier as high as $1.7 k_B T$ prevented the large spheres from touching one another. Furthermore, the rate at which two large particles came into contact was much slower than expected, even after the observed free-energy barrier and the increase of the bulk viscosity owing to an increase in ϕ_S were accounted for.

Figure 5 demonstrates the origin of the entropic repulsion: A shell of small spheres surrounds a larger sphere. Owing to this layering the large spheres must squeeze out all the intervening small spheres to approach one another. Because these
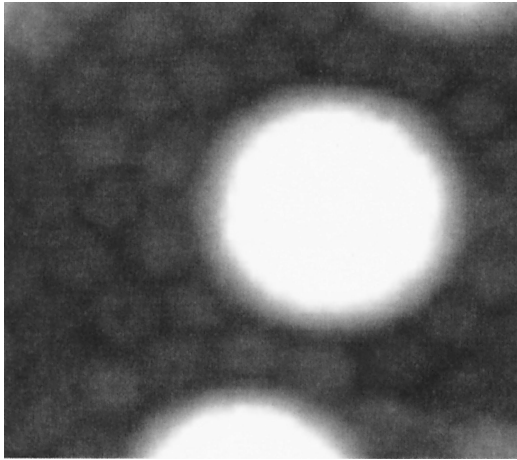
Fig. 5. Confocal microscope image of a pair of 2.1-μm-diameter spheres surrounded by 0.5-μm-diameter spheres. The pronounced layering of the smaller spheres gives rise to the depletion repulsion. The volume fractions of the larger and the smaller spheres are 0.24 and 0.28, respectively.
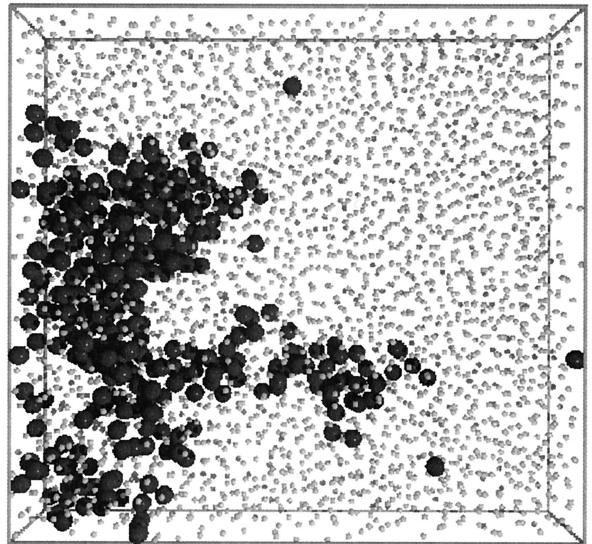

Fig. 6. Locations of the fast particles (large spheres, drawn to scale) and the other particles (smaller spheres, not to scale) in a supercooled fluid sample ($\phi = 0.56$). This is a snapshot from the sample in Fig. 7(a) below at $t = 40$ min.

small particles are densely packed in the gap, it takes an anomalously long time for them to diffuse out of the way. This observation also agrees with simulations of structural relaxations in binary liquids.[28] The structural relaxations were much slower for a large concentration of small particles and a few large particles than for a large concentration of large particles with a few small ones.

The layering of the small particles can be explained by consideration of the volume that is accessible to the particles' centers of mass (hence, their entropy), which tends toward a maximum. Each small particle that is located a short distance away from the wall (with its surface less than a diameter away) creates a small region from which all other particles are excluded. If this particle moves closer to the wall some of this space becomes accessible to the other particles. For this reason hard spheres tend to form layers along surfaces.[29,30] Here, the confocal microscope's capability of distinguishing clearly the ordering of the small spheres about the large ones contributes to a useful description of the structure of a binary system.

C. Colloidal Glass

We also used confocal microscopy to examine the microscopic dynamics of concentrated colloidal suspensions near their glass transition. Hard spheres form crystals when the volume fraction ϕ exceeds the freezing point of $\phi_f = 0.494$.[10] Even when $\phi > \phi_f$, however, the sample can remain in a metastable supercooled-fluid state for times much longer than the experimental time scale. Further, highly concentrated samples do not crystallize at all. The glass transition is defined by the empirical observation that samples with $\phi > \phi_{glass}$ do not form crystals within an experimentally accessible time (>1 year). For the suspensions used in these studies $\phi_{glass} \approx 0.58$. Supercooled-fluid and glass samples are in a metastable, disordered state whose structure factor

is not distinguishable from that of the thermally stable fluid phase. Particles in such samples no longer diffuse freely; instead, they spend much of their time trapped in cages formed by their neighboring particles. Occasionally these cages rearrange themselves, allowing particles to move throughout the sample, albeit on slow time scales. On time scales (>days) longer than the time during which the experiment is performed these mobile particles become responsible for the growth of crystals; a full understanding of the dynamics of dense fluids therefore requires direct measurements of these individual motions. Furthermore, a complete understanding of the glass transition requires measurements of these motions as the glass transition is approached. The existence of the hard-sphere glass transition has been known for decades,[31,32] and the colloidal realization of such a system has been studied since the 1980s.[10,33,34] However, the motions of the individual particles were only recently measured for the first time.[3,5]

Strikingly, the structural rearrangements in a dense, supercooled fluid near ϕ_{glass} are spatially inhomogeneous, as can be seen from Fig. 6. This figure shows, at an instant in time, the locations of all fast particles (shown as large spheres), which are defined as those particles whose displacements in the time interval Δt^* (=1000 s) exceeds a cutoff of 0.27 μm. The time scale and the length scale are chosen to highlight particles that are undergoing cage rearrangements (for details, see Ref. 3). All the particles in the experiment are of the same size, but in the figure, the fast particles are represented as large spheres, and the other particles as smaller spheres. At different initial times, different particles are fast, but these rearranging particles are always localized in clusters. The average size of the clusters grows as
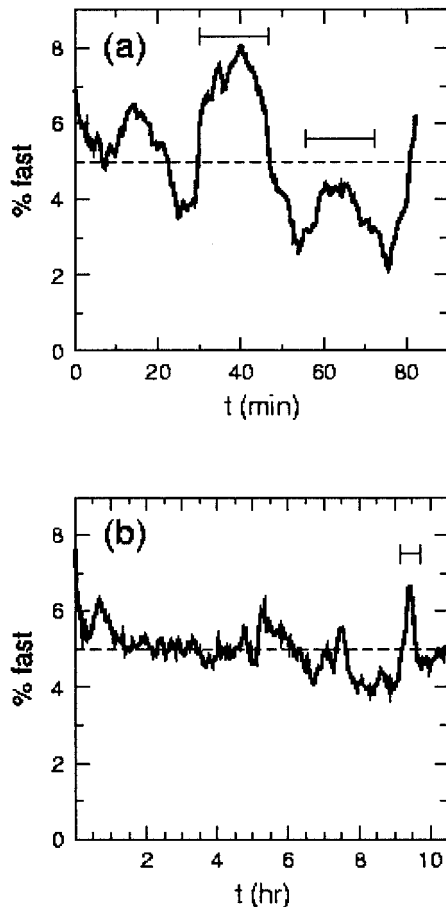
Fig. 7. Measured percentage of the sample that is fast as a function of time for (a) a supercooled fluid ($\phi = 0.56$) and (b) a colloidal glass ($\phi = 0.60$). The definition of fast is chosen to select, on average, the 5% of particles with the largest displacements during time interval Δt^*. Horizontal bars, time scale Δt^*; dashed lines, time-averaged population of fast particles. The large fluctuations in the supercooled sample are not seen in the glass sample.

ϕ_{glass} is approached from below. For glassy samples, however, the clusters are dramatically smaller.[3]

The structural relaxation is temporally inhomogeneous as well. At any given instant in time the fraction of particles that meets the definition of fast varies. The fluctuations in this fraction are shown in Fig. 7 for a supercooled-fluid sample [Fig. 7(a), $\phi < \phi_{\text{glass}}$] and for a glassy sample [Fig. 7(b), $\phi > \phi_{\text{glass}}$]. Whereas the average is constrained to be 5%, there are large fluctuations about this average in the case of the supercooled fluid. These fluctuations are larger than $\sqrt{N}$ fluctuations: The imaged volume contains at most ~ 5000 particles, and 5% of this 5000 is 250 particles; thus $\sqrt{N}$ fluctuations would be $\sqrt{250} \approx 16$, implying that roughly $5.0\% \pm 0.3\%$ of the imaged sample should be fast. As one can see from Fig. 7(a), however, the fluctuations are an order of magnitude larger. The horizontal bars indicate the time scale Δt^* that we use to define fast particles and that shows that the duration of the largest fluctuations is roughly the same as Δt^*. For the colloidal glasses, the spatial behavior is significantly more homoge-

neous[3] than for the supercooled fluid, and the temporal fluctuations likewise are reduced, as shown in Fig. 7(b). Both the spatial and the temporal inhomogeneities therefore appear to be signatures of the glass transition. It is impossible to detect these features in a conventional light-scattering experiment, which measures only spatial and temporal averages.

4. Conclusion

We have discussed the use of a confocal microscope for measuring the three-dimensional positions of 10^4 particles within a few seconds. The advantages of obtaining this unique information were described by use of examples of colloidal gels, concentrated binary colloidal fluids, and colloidal glasses. In these three examples the structure and the dynamics are heterogeneous. A scattering measurement of the average properties, therefore, provides an incomplete view. The morphology of the gels was discussed in terms of the number of bonds per particle and of the presence of chains and loops in the structure. Pronounced layering of small particles was observed in the dense binary suspension, providing a direct explanation of the previously observed depletion repulsion. Finally, in the glass samples the mobilities of the individual particles were found to be spatially and temporally inhomogeneous, with fluctuations increasing as the glass transition was approached.

References

1. T. Wilson and B. R. Masters, "Confocal microscopy," Appl. Opt. **33,** 565–566 (1994).
2. A. van Blaaderen and P. Wiltzius, "Real-space structure of colloidal hard-sphere glasses," Science **270,** 1177–1179 (1995).
3. E. R. Weeks, J. C. Crocker, A. C. Levitt, A. Schofield, and D. A. Weitz, "Three-dimensional direct imaging of structural relaxation near the colloidal glass transition," Science **287,** 627–630 (1999).
4. M. H. Chestnut, "Confocal microscopy of colloids," Curr. Opin. Colloid Interface Sci. **2,** 158–161 (1997).
5. W. K. Kegel and A. van Blaaderen, "Direct observation of dynamical heterogeneities in colloidal hard-sphere suspensions," Science **287,** 290–292 (2000).
6. U. Dassanayake, S. Fraden, and A. van Blaaderen, "Structure of electrorheological fluids," J. Chem. Phys. **112,** 3851–3858 (2000).
7. K. H. Lin, J. C. Crocker, V. Prasad, A. Schofield, D. A. Weitz, T. C. Lubensky, and A. G. Yodh, "Entropically driven colloidal crystallization on patterned surfaces," Phys. Rev. Lett. **85,** 1770–1773 (2000).
8. A. van Blaaderen, "Imaging individual particles in concentrated colloidal dispersions by confocal scanning light microscopy," Adv. Mater. **5,** 52–54 (1993).
9. N. A. M. Verhaegh, D. Asnaghi, and H. N. W. Lekkerkerker, "Transient gels in colloid–polymer mixtures studied with fluorescence confocal scanning laser microscopy," Physica A **264,** 64–74 (1999).
10. P. N. Pusey and W. van Megen, "Phase behavior of concentrated suspensions of nearly hard colloidal spheres," Nature **320,** 340–342 (1986).

11. W. C. K. Poon, J. S. Selfe, M. B. Robertson, S. M. Ilett, A. D. Pirie, and P. N. Pusey, "An experimental study of a model colloid–polymer mixture," J. Phys. France **3,** 1075–1086 (1993).

12. W. C. K. Poon, "Phase separation, aggregation and gelation in colloid–polymer mixtures and related systems," Curr. Opin. Colloid Interface Sci. **3,** 593–599 (1998).

13. S. Asakura and F. Oosawa, "Interaction between particles suspended in solutions of macromolecules," J. Polym. Sci. **33,** 183–191 (1958).

14. J. C. Crocker, J. A. Matteo, A. D. Dinsmore, and A. G. Yodh, "Entropic attraction and repulsion in binary colloids probed with a line optical tweezer," Phys. Rev. Lett. **82,** 4352–4355 (1999).

15. J. C. Crocker and D. G. Grier, "Methods of digital video microscopy for colloidal studies," J. Colloid Interface Sci. **179,** 298–310 (1996).

16. W. C. K. Poon, A. D. Pirie, and P. N. Pusey, "Gelation in colloid–polymer mixtures," Faraday Discuss. **101,** 65–76 (1995).

17. A. H. Krall and D. A. Weitz, "Internal dynamics and elasticity of fractal colloidal gels," Phys. Rev. Lett. **80,** 778–781 (1998).

18. P. N. Segre, V. Prasad, A. B. Schofield, and D. A. Weitz, "Glass-like kinetic arrest at the colloidal gelation transition," Phys. Rev. Lett. **86,** 6042–6045 (2001).

19. P. Meakin, "Formation of fractal clusters and networks by irreversible diffusion-limited aggregation," Phys. Rev. Lett. **51,** 1119–1122 (1983).

20. R. Jullien and R. Botet, *Aggregation and Fractal Aggregates* (World Scientific, Singapore, 1987).

21. M. Lach-hab, A. E. Gonzalez, and E. Blaisten-Barojas, "Concentration dependence of structural and dynamical quantities in colloidal aggregation: computer simulations," Phys. Rev. E **54,** 5456–5462 (1996).

22. M. Broide and R. Cohen, "Experimental evidence of dynamic scaling in colloidal aggregation," Phys. Rev. Lett. **64,** 2026–2029 (1990).

23. D. A. Weitz and M. Y. Lin, "Dynamic scaling of cluster-mass distributions in kinetic colloid aggregation," Phys. Rev. Lett. **57,** 2037–2040 (1986).

24. D. A. Weitz, J. S. Huang, M. Y. Lin, and J. Sung, "Limits of the fractal dimension for irreversible kinetic aggregation of gold colloids," Phys. Rev. Lett. **54,** 1416–1419 (1985).

25. L. Cipelletti, S. Manley, R. C. Ball, and D. A. Weitz, "Universal aging features in restructuring of fractal colloidal gels," Phys. Rev. Lett. **84,** 2275–2278 (2000).

26. A. A. Potanin and W. B. Russel, "Fractal model of consolidation of weakly aggregated colloidal dispersions," Phys. Rev. E **53,** 3702–3709 (1996).

27. W. Wolthers, D. van den Ende, V. Breedveld, M. H. G. Duits, A. A. Potanin, R. H. W. Wientjes, and J. Mellema, "Linear viscoleastic behavior of aggregated colloidal dispersions," Phys. Rev. E **56,** 5726–5733 (1997).

28. S. Sinha, "Dynamic structure factors of a dense mixture," Phys. Rev. E **49,** 3504–3507 (1994).

29. B. Gotzelmann, A. Haase, and S. Dietrich, "Structure factor of hard spheres near a wall," Phys. Rev. E **53,** 3456–3467 (1996).

30. D. J. Courtemanche, T. A. Pasmore, and F. van Swol, "A molecular dynamics study of prefreezing hard spheres at a smooth wall," Mol. Phys. **80,** 861–875 (1993).

31. L. V. Woodcock, "Glass-transition in the hard-sphere model and the Kauzmann paradox," Ann. N. Y. Acad. Sci. **371,** 274–298 (1981).

32. B. J. Alder and T. E. Wainright, "Studies in molecular dynamics. 2. Behavior of a small number of elastic spheres," J. Chem. Phys. **33,** 1439–1451 (1960).

33. E. Bartsch, V. Frenz, S. Moller, and H. Silescu, "Colloidal polystyrene micronetwork spheres—a new mesoscopic model of the glass transition in simple liquids," Physica A **201,** 363–371 (1993).

34. W. van Megen and S. M. Underwood, "Glass transition in colloidal hard spheres: measurement and mode coupling–theory analysis of the coherent intermediate scattering function," Phys. Rev. E **49,** 4206–4220 (1994).